International Journal of Automotive Technology, Vol. 23, No. 3, pp. 855–865 (2022)
DOI 10.1007/s12239–022–0076–0

pISSN 1229–9138/ eISSN 1976–3832

COMPUTATIONAL STUDY ON THE FRICTIONAL POWER LOSS REDUCTION OF PISTON RING WITH LASER SURFACE TEXTURING ON THE CYLINDER LINER

Siyoul Jang*

School of Automotive Engineering, Kookmin University, Seoul 02707, Korea

(Received 19 April 2021; Revised 31 May 2021; Accepted 1 June 2021)

ABSTRACT–Hydrodynamic lubrication is simulated under the contact conditions that the direction of contact velocity reverses with a sudden high applied load in the contact of piston top ring and cylinder liner. Hydrodynamic lubrication film formation and pressure between piston ring and cylinder liner at the top dead center (TDC) location are investigated in detail because most friction loss and wear damage happen at this location due to the thin-film thickness resulting from the slow-down and reversal contact velocities as well as high applied load. The surface roughness on the cylinder liner by the honing process that is similar scale to the lubrication film thickness at TDC location is considered. Around the TDC location, laser surface textured (LST) surface that is larger scale than the surface roughness is designed for the favorable film formation. These two surface roughness parameters are simulated to study the effects of favorable film formation and less frictional loss of piston top ring at TDC location where most of damage and friction loss occur. Frictional power loss and minimum film thickness of the cylinder surfaces of the honed roughness are compared with those of patterned designs.

KEY WORDS : Transient lubrication film, Laser surface texture (LST), Top ring, Hydrodynamic lubrication, Top dead center (TDC), Asperity contact

NOMENCLATURE

A_a	: asperity contact area, m^2
c	: piston ring profile height, m
d	: depth of LST pattern, m
F_{fasp}	: friction of asperity contact, N
F_{fhyd}	: shear resistance of the hydrodynamic lubrication film, N
$F_{ring\ tension}$	: piston ring tension, N
$F_2(\chi)$	: statistical function of the lubricant film ratio
$h(x, y, t)$	: lubrication film thickness, m
$h_0(x, y, t)$	: minimum film thickness, m
$h_c(x, y, t)$	: lubrication film thickness by the piston ring profile, m
$h_d(x, y, t)$	: lubrication film thickness by the LST geometry, m
$h_s(x, y, t)$	: lubrication film thickness by surface roughness, m
L	: length of the LST pattern, m
L_p	: pitch of the LST pattern, m
l_{pr}	: width of the piston ring, m
p_{hyd}	: hydrodynamic pressure, Pa
p_{asp}	: asperity contact pressure, Pa
p_c	: vapor pressure of the lubricant, Pa
p_{comb}	: combustion pressure, Pa
R_a	: surface roughness, m
R_c	: radius of the crank shaft rotation, m
U	: sliding velocity, ms^{-1}
W	: width of the LST pattern, m
W_a	: asperity contact load, N
x_c	: coordinate in the ring profile, m
x_d	: coordinate in the LST pattern, m
$x_p(\theta)$	: piston's displacement, m
$\dot{x}_p(\theta)$	: piston's velocity, ms^{-1}
z	: asperity height, m
μ	: lubricant viscosity, Pa·s
ρ	: lubricant density, $kg{\cdot}m^{-3}$
θ	: volume fraction of the fluid
β	: radius of curvature of an asperity, m
η	: asperity density per unit surface area, m^{-2}
σ	: average asperity height, m
τ_0	: limiting Eyring shear stress, Pa
ς	: pressure-induced shear strength of asperities

1. INTRODUCTION

Piston ring plays a vital role in applications such as the sealing of combustion gas, heat transfer to cylinder liner, control of oil transportation on the cylinder liner, and lubricated movement of the piston. It gets exposed to severe contact conditions during the piston's stroke movement, especially in the region of top dead center (TDC) during the

*Corresponding author. e-mail: jangs@kookmin.ac.kr

power stroke. It undergoes a reversal in the direction of movement with zero contact velocity as well as high load due to the combustion pressure at the TDC. During the reversal movement of the piston ring, the lubricant film becomes very thin (down to surface roughness level) and experiences large frictional loss and wear. If the lubricant supply is not enough to maintain the lubricant film against the applied load on the piston ring, it comes in direct contact with the surface of the cylinder, resulting in large surface damages and frictional power loss.

To avoid this type of frictional contact of the piston ring, continuous lubricant supply is necessary around the TDC location even though the oil ring scrapes down the lubricant on the cylinder liner to lessen the oil consumption. Plateau-valley honing surface roughness is one of the handling methods for the continuous lubricant supply by trapping the oil with a little oil consumption. Refined honing surface roughness according to honing angles and deep groove/valley distribution (Knopf *et al*., 1998; Chen and Tian, 2008) is suggested as a more advanced method for controlling lubricant supply on the interface between a piston ring and cylinder liner.

Many analytical investigations of piston ring lubrication concerning film formation have been performed taking into account the surface roughness. The surface roughness effect is statistically included in the surface pattern orientations based on Patir and Cheng's average flow method (Patir and Cheng, 1979). Most of these studies (Akalin and Newaz, 2001; Jocsak *et al*., 2006) on lubricant film analysis with surface roughness effects of cylinder honing processes are based on the average flow factors. Hu *et al*. (2018) suggested a homogenized Reynold's equation to study the effect of surface roughness on the lubrication and oil transportation due to the honing process for surface patterns with crosshatch angled plateau-valley shape. Some studies on the lubrication film thickness have deterministically employed the measured surface roughness values for calculating the hydrodynamic lubrication film pressures differently from those of the average flow methods. Deterministic method with the measured data of the surface roughness offers the advantage of a more-detailed investigation of the film formation characteristics under the thin-film thickness on the TDC area and can suggest better honing process regarding surface roughness scale and honing angle, especially for the TDC location where most of friction loss and surface damage occur (Mezghani *et al*., 2013; Li *et al*., 2008).

Besides honing surface roughness optimization for the trapped oil supply mechanism, more active oil supply on the cylinder liner around the TDC location was devised via laser surface texturing (LST) with various geometries such as circles, ellipses, and rectangles (Etsion and Sher, 2009; Zhan and Yan, 2012; Vladescu *et al*., 2015). LST pattern takes more preferable advantages that the propagation velocity of the local oil film reinforcement increases due to the transient lubrication phenomena induced by the surface cavity structure passed through the contact area than plateau-valley honing pattern (Krupka *et al*., 2011). Such transient lubrication due to the LST on the cylinder liner surface is different from the honing surface roughness that has less scale (R_a = ~0.3 μm and honing groove depth of several micrometers) than the LST pattern depth (20.0 μm) and actively makes the lubrication regime from the boundary to hydrodynamic lubrication even in unidirectional sliding contact. If the contact speed has a reversal movement, the transient film thickness increases by the LST on the contact surface, especially in the TDC location. Based on this type of transient phenomena, lubrication film is more reformed, even before and after the TDC where the contact velocity is suddenly in reversal mode under extremely high applied load. An experimental study (Carden *et al*., 2006) on piston ring friction under real engine operation conditions revealed that during the power stroke, the frictional force between the piston ring and cylinder liner is very high, while only rig tests without the real engine ignition revealed repeated similar frictional modes as the stroke continues (Vlădescu *et al*., 2017). The experiments indicated that high load caused the lubrication film to be very thin and its effect on the friction and wear was as large as the reversal velocity mode.

LST can form on either moving (Etsion and Sher, 2009; Gadeschi *et al*., 2012; Usman and Park, 2017) or stationary part (Checo *et al*., 2014) for increased load capacity via the transient lubrication mechanism. Calculation domain for the LST on the moving part, i.e., on the piston ring, is generally fixed as the contact surface of the piston ring. It is relatively easy to obtain stable converged computation because the geometrical shape of the computational domain is fixed. However, the shape of the geometrical contact of LST on the stationary surface (on the cylinder liner) changes as the contact surface of the piston ring moves. It provides more actively transient film formation even under the zero contact velocity at the moment of reversal mode of contact velocity; therefore, the calculation domain for the LST on the stationary surface is more complicated and requires much smaller time step in the calculation.

Modeling of the moving LST of thin rectangular transverse groove shape around some region of TDC location, including honing surface roughness, is applied for the frictional force analysis of the top ring with combustion engine pressure variation during a cycle. Modeling of the computational domain describes the contact of piston ring sliding on the LST stationary surface (LST surface), which always generates transient conditions of hydrodynamic lubrication contact. The calculation results show that fuel consumption is less compared to that of non-LST on the cylinder liner with only honing surface roughness (smooth surface).

2. MODELING OF PISTON STROKE MOVEMENT AND PISTON RING

Piston ring movement depends on the piston's motion that has a stroke displacement from the TDC to the BDC. Detailed motion of the piston ring, such as axial and twist movements in the ring groove, is not included in this work, and it is considered to have the same velocity as that of piston's primary movement. Figure 1 shows the piston's primary movement from the TDC to BDC and its velocity variation during a cycle. Combustion pressure, p_{hyd}, is applied on the backside of the piston ring that makes contact with the cylinder liner surface. The piston's displacement $x_p(\theta)$ and velocity $\dot{x}_p(\theta)$ are described in Equations (1) and (2).

Along with the combustion pressure at the top land of a piston, inter-ring pressure in the second land needs to be calculated according to the gas flow mechanism (Turnbull *et al*., 2020; Morris *et al*., 2016) during a cycle to impose boundary conditions on the computation of hydrodynamic lubrication pressure between the piston ring and cylinder liner. The second land pressures vary according to the combustion

$$x_p(\theta) = \sqrt{L_{cr}^2 - R_c^2 sin^2\theta} + R_c cos\theta \tag{1}$$

$$\dot{x}_p(\theta) = -R_c sin\theta \frac{d\theta}{dt} - \frac{R_c^2 cos\theta sin\theta}{\sqrt{L_{cr}^2 - R_c^2 sin^2\theta}} \frac{d\theta}{dt} \tag{2}$$

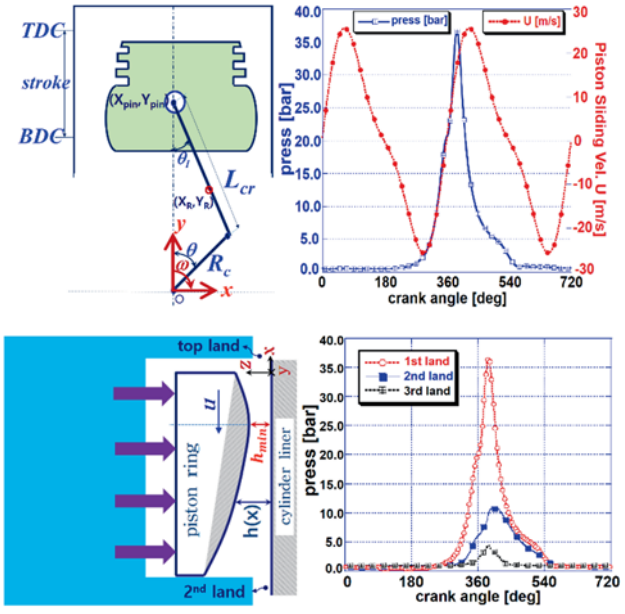

Figure 1. Piston's primary movement in the cylinder liner and piston ring's applied load by combustion pressure at 3000 rpm under full load.

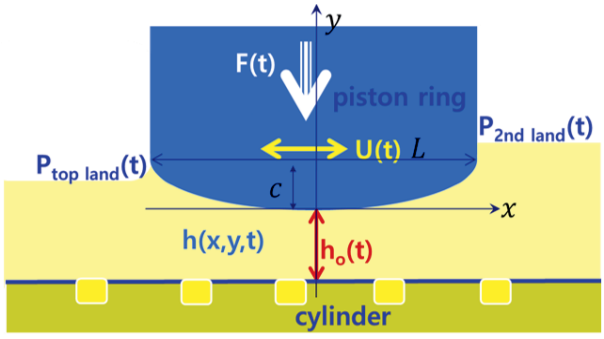

Figure 2. Piston ring profile and boundary conditions for the hydrodynamic lubrication computation with top and second land pressures.

pressures, ring gap size, and shape during a cycle; the hydrodynamic lubrication pressures are computed depending on boundary pressures, one side of top land pressure of combustion pressure, and the other side of second land pressure. For simplicity, the piston ring profile is considered to be a parabolic curve and the film is considered under fully flooded conditions; however, the ring profile may have various forms depending on the fuel economy and durability performance of an engine (Figure 2).

3. SURFACE ROUGHNESS AND LST ON CYLINDER LINER

LST forms on the cylinder liner surface where the piston ring slides. Figure 3 shows the cylinder surface roughness and LST pattern shape studied in this work. The LST forms at only some regions of the stroke around the TDC (crank angle, CR 10 ~ 45°) because most of the severe lubrication occurs around the TDC. Surface roughness (R_a = ~ 0.3 μm) is simulated, and a honing pattern (ridge depth = ~ 1.5 μm) with a 45° angle is made. The LST pattern on the honing surface has a length, width, and parabolic depth of 3.0 mm, 60.0 μm, and 20.0 μm, respectively. The LST pattern appears repeatedly at distances of L_p = 2.0 and L = 5.0 mm in the sliding and circumferential directions, respectively.

The computational domain for the hydrodynamic lubrication is selected as 5.0-mm width and piston ring width (l_{pr} = 1.2 mm) along with the stroke movement. Two-dimensional pressure and film thickness are computed for the periodic boundary condition at both sides of the selected LST band, which is repeated in the circumferential direction on the cylinder surface (Figure 3). The film thickness on the surface of the LST pattern is relatively larger than any other region of honing plateau-valley and the surface roughness itself.

The film thickness of the LST pattern is denoted as $h_d(x, y, t)$ of parabolic depth, deterministic surface roughness $h_s(x, y, t)$, and piston ring profile $h_c(x, y, t)$.

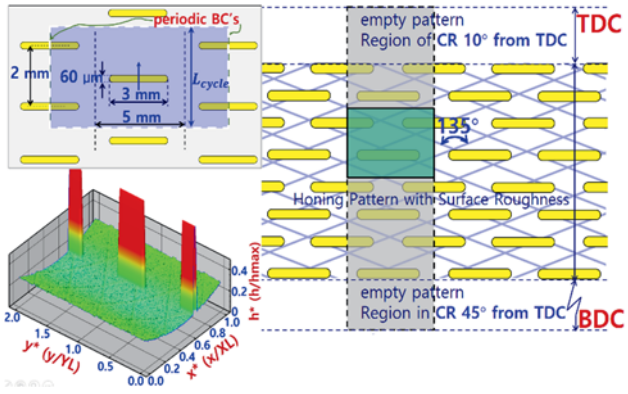

Figure 3. LST pattern at a depth of 20.0 μm on cylinder liner around TDC from crank angle of 10 ~ 45° from TDC and honed surface roughness R_a = 0.3 μm, honing groove depth = 1.5 μm, honing ridge angle = 45°.

Therefore, the hydrodynamic lubrication film thickness at a certain time during the piston's stroke movement is given by $h(x, y, t) = h_c(x, y, t) + h_s(x, y, t) + h_d(x, y, t)$. As the piston ring moves from the TDC to BDC, the film thickness varies abruptly depending on the existence of the LST in the contact region along with the applied load and velocity. Even if the sliding velocity and applied load are constant, the LST changes the contact geometry as the piston ring slides. It yields transient lubrication phenomena, and hydrodynamic lubrication is more favorably developed with LST. In this work, for the computation of hydrodynamic lubrication film thickness and pressure, the varying contact geometry with LST are considered and the time step for the transient lubrication behaviors is set to be small enough to obtain a stable converged solution. Considering the varying contact geometry of the LST pattern as the piston ring slides, the transient hydrodynamic pressure is very sensitively affected by the LST pattern; as such, the film load capacity reflects the applied load, contact velocity, and LST pattern on the contact geometry. Different from the LST pattern on the moving part, such as the piston ring, the film thickness variation vibrates on a very small scale (Vlădescu *et al*., 2015; Checo *et al*., 2014). If the piston ring with the LST pattern slides on cylinder liner, then small vibration in the film thickness variation does not exist, and it is affected mainly by the applied load and sliding velocity (Etsion and Sher, 2009; Turnbull *et al*., 2020).

The parabolic piston ring profile is given by

$$h_c(x_c, y) = \frac{c\,(x_c)^2}{\left(\frac{L}{2}\right)^2} \tag{3}$$

where $x_c = x_p \times int(x_p, l_{pr}) - x_{c0}$, $x_{c0} = \mathrm{mod}(x_p, l_{pr})$ and $-L/2 \le x_c \le L/2$, and the film thickness of the LST is given by a parabolic shape depth as follows:

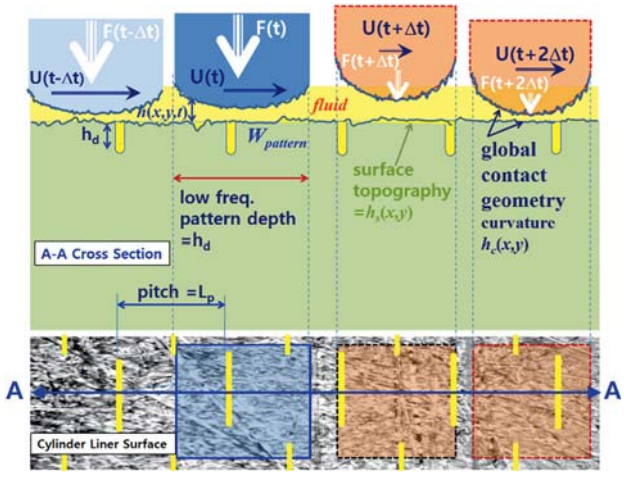

Figure 4. Cylinder liner surface with LST and variation in the contact geometry as the piston ring's stroke from the TDC to BDC (LST depth = 20.0 μm, R_a = 0.3 μm honing groove depth = 1.5).

$$h_d(x_d, y) = \frac{d\,x_d^2}{\left(\frac{W}{2}\right)^2} \tag{4}$$

where $-W/2 \le x_d \le W/2$ and d is the LST pattern depth.

The film shape changes as the piston ring slides on the cylinder liner surface due to the LST pattern, even without any variations in the contact load and speed. The LST pattern on the stationary part inherently results in the transient hydrodynamic lubrication phenomena (Figure 4).

The hydrodynamic pressure for the lubrication between the piston ring and cylinder liner can be explained using the Reynolds equation. Because film thickness includes deterministic surface roughness, LST structure, and piston ring profile, the computation of the hydrodynamic lubrication phenomena needs to be based on the physical conditions corresponding to the occurrence of cavitation in the hydrodynamic film thickness computation. The mass conservation law is fully applied and is reflected in the governing Equation (5). The film model is considered as fully flooded condition (Liu *et al*., 2019). Many other experimental or numerical studies (Vlădescu *et al*., 2017; Liu *et al*., 2019) have shown the differences in the computational results between flooded and starved boundary conditions. However, friction and wear tendency of the lubrication performance with respect to the minimum film thickness value is similar under each flooded or starved condition.

In this work, similar procedures as those employed in previous studies (Ma *et al*., 1996) have been used for the computational process of the load capacity performances of the hydrodynamic lubrication. The cavitation effects of the mass conservation law with Poiseuille and Couette flows are considered because the contact geometry includes textured

surfaces, which is somehow larger scale than the honed surface roughness. The computational domain for the hydrodynamic lubrication behavior moves as the piston ring makes the stroke movement, and it is selected for the repeatable sector with repeated boundary conditions at both sides in the circumferential direction of the cylinder liner and piston ring's width along the stroke direction.

$$\frac{(\Delta \dot{m}_x)^p}{\Delta x} + \frac{(\Delta \dot{m}_y)^p}{\Delta y} = -\frac{(\Delta \dot{m}_x)^c}{\Delta x} + \rho \frac{\partial(\theta h)}{\partial t} \tag{5}$$

$$\text{where, } \frac{(\Delta \dot{m}_x)^p}{\Delta x} = \frac{1}{\Delta x}\left[\frac{\rho h^3}{12\mu}\left(\frac{\partial p}{\partial x}\right)\right] , \tag{6}$$

$$\frac{(\Delta \dot{m}_y)^p}{\Delta y} = \frac{1}{\Delta y}\left[\frac{\rho h^3}{12\mu}\left(\frac{\partial p}{\partial y}\right)\right] , \tag{7}$$

$$(\Delta \dot{m}_x)^c = \rho \frac{U}{2}\left\{\theta_{i-1,j} h_{i-1,j}\left(1 - g_{i-1,j}\right) + g_{i-1,j} h_{i-1,j} + g_{i-1,j} g_{i,j}\left(\frac{h_{i,j} - h_{i-1,j}}{2}\right)\right\} , \tag{8}$$

$$\rho \frac{\partial(\theta h)}{\partial t} = \rho \theta_{i,j}\left\{\left(\frac{h_{i,j}^{(t)} - h_{i,j}^{(t-1)}}{\Delta t}\right) + h_{i,j}\left(\frac{\theta_{i,j}^{(t)} - \theta_{i,j}^{(t-1)}}{\Delta t}\right)\right\} , \tag{9}$$

$$p = g_{i,j} p_{hyd\,i,j} + (1 - g_{i,j}) p_c . \tag{10}$$

Two variables—hydrodynamic pressure p_{hyd} and auxiliary volume fraction of fluid θ — need to be manipulated in the computation, and they should satisfy the two conditions for the converged solution (Ma *et al*., 1996; Chong *et al*., 2011):

$$\theta \geq 1 \; and \; g = 1, if \; p_{hyd} > p_c , \tag{11}$$

$$p_{hyd} = p_c \; and \; g = 0, \; if \; \theta < 1. \tag{12}$$

4. ASPERITY CONTACT MODEL AND COMPUTATION PROCESS

The clearance between the piston ring and cylinder liner becomes very small for large applied loads or relatively small contact velocities. This type of lubrication behavior happens around the TDC location. Under this contact condition, direct contact pressure is generated between the piston ring and cylinder liner. Asperity on the rough surface roughness makes real contact pressure and the hydrodynamic lubrication pressure is generated when the film thickness is large enough to separate two contact surfaces. The contact pressure reflects the density and tip curvature of asperity of the surface roughness and can be described using the following equations. The LST pattern forms deep in the surface roughness level, and most of the contact pressure occurs due to the honed surface roughness pattern. The asperity contact pressure p_{asp} can be given by the following equation (Liu *et al*., 2019):

$$p_{asp} = \frac{16\sqrt{2}}{15}\pi(\sigma\beta\eta)^2 E \frac{\sqrt{\sigma}}{\beta} F\left(\frac{h(z)}{\sigma}\right) \tag{13}$$

where $F(\chi) = \frac{1}{\sqrt{2\pi}}\int_0^\infty (s - \chi)^{2.5} exp\,(-\frac{s^2}{2}) ds.$

Both asperity contact pressure p_{asp} and hydrodynamic fluid pressure p_{hyd} support the two applied forces. One is the pressure on the backside of the top ring, which is considered as the first land pressure. The other is the ring tension force $F_{ring\ tension}$ (12.6 N). The force balance is checked with the Equation (14). All the asperity contact pressures are based on the deterministic values of the surface roughness data for the calculation domain as follows:

$$\int p_{hyd}\, dA + \int p_{asp}\, dA = \int\int p_{comb}\, dA\; dA + F_{ring\ tension} \tag{14}$$

Frictional force due to the contact between the piston ring and cylinder liner comprises the shear resistances of hydrodynamic lubrication film, F_{fhyd}, and the friction of asperity contact, F_{fasp}.

$$F_{fhyd} = \int \left(\frac{h}{2}\frac{\partial p}{\partial x} - \mu \frac{U}{h}\right) dA \tag{15}$$

$$F_{fasp} = \tau_0 A_a + \varsigma W_a \tag{16}$$

where $A_a = \pi^2(\alpha\beta\eta)^2 A F_2(\chi)$, A is the apparent contact area, and $F_2(\chi)$ is a function given by Greenwood and Tripp (1970). τ_0 is the limiting Eyring shear stress (2 MPa), and ς is the pressure-induced shear strength of asperities (0.11 in this computation) (Liu *et al*., 2019; Kong and Jang, 2020).

The hydrodynamic lubrication analysis is considered in the computational process. If the contact film thickness is below a certain lower limit (e.g., h/σ = 4.0), then asperity contact pressure is calculated based on the film thickness. The applied load balances by the backside pressure on the piston ring and ring tension are checked with the reaction forces from both the hydrodynamic lubrication pressure and the asperity contact pressure. If these do not match, then the contact film thickness is adjusted until the load balance is satisfied. Once the converged load balance is obtained at a certain crank angle, the frictional force from the fluid film and asperity contact pressures are calculated. This computation is processed during the engine cycle, including intake, compression, power, and exhaust strokes, and the

time step needs to be small (in terms of crank angle 1°) so that the computational stability is achieved.

5. COMPUTATIONAL RESULTS

Computational results are obtained for the comparison of the hydrodynamic pressure, minimum film thickness, frictional force, and power loss for the contact of the piston ring between the smooth (honing surface) and LST surfaces (LST pattern on honing surface). Variations in the load capacity of the hydrodynamic lubrication on the LST surface during a cycle stroke movement of the piston ring are shown. Computational domain is meshed into 801 by 101 for the physical domain of l_{pr} = 1.2 mm in the x direction of piston ring movement and L = 5.0 mm for the repeated circumferential y direction of the LST pattern; these represent the width and repeated pattern length, respectively, of the piston ring.

The same applied load on the piston ring and contact velocity between the piston ring and cylinder liner are set for the smooth and LST surfaces for comparison (Figure 1). The variations in the minimum film thickness are almost the same except for the stroke region at crank angle of 10 ~ 45° (315 ~ 350°, 370 ~ 405°, and 675 ~ 710°; Figure 5) where the LST pattern is observed on the cylinder liner (Figure 5). Although the contact behavior at the exact TDC location is very severe, the LST pattern is a little distant from the TDC to provide appropriate oil supply into the TDC location because it might increase the consumption of lubricant that flows directly into the combustion chamber. Computational results show that the minimum film thickness increases mainly in the region of the LST-patterned locations. Owing to the LST shape in the control volume as the piston ring passes, changing of control volume generates transient hydrodynamic lubrication pressure; this enhances the load capacity of the lubrication film. Therefore, the minimum film thickness increases; this reduces the possibility of mixed lubrication with oil supply at the TDC location between the piston ring and cylinder liner. Figure 5 shows the increased variations in the minimum film thickness in the LST-patterned region on the cylinder liner. If the LST pattern is placed on the moving surface of a piston ring, there is no variation in the film thickness. In this case, the enhancement of film thickness is less than that in the LST pattern on the stationary surface (Gadeschi *et al.*, 2012). Most of the frictional loss on the piston ring occurs at the TDC location with thin-film lubrication, causing the mixed lubrication. From the computational results, it can be stated that this type of LST on the cylinder liner can reduce the possibility of mixed lubrication by enhancing the lubrication film.

Hydrodynamic pressures are compared in the cases of smooth and LST surfaces at selected crank angles (Figures 6 ~ 8). Film thickness changes over the contact area are shown

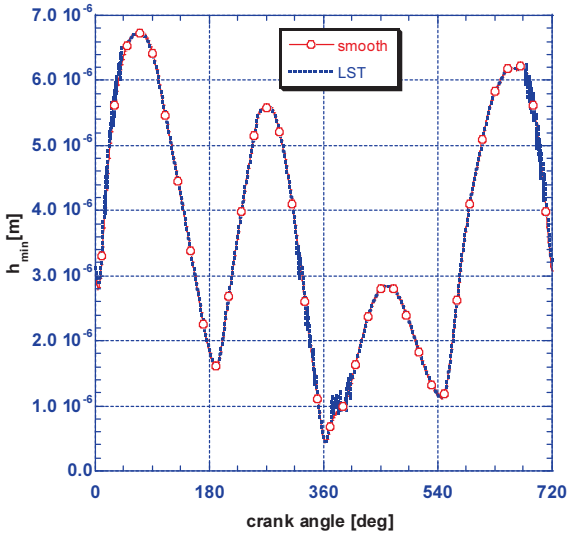

(a) Film thickness during a cycle

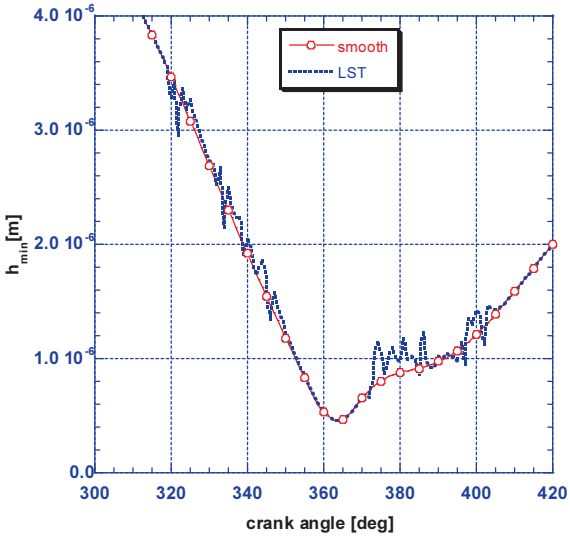

(b) Film thickness selected power stroke crank angle range

Figure 5. Variations in the film thicknesses between smooth and LST cylinder surfaces at 3000 rpm under full load.

shown in Figure 7 for the LST-patterned surface and Figure 9 for smooth surface, respectively. Hydrodynamic pressure with the LST pattern has a relatively higher distribution over the contact area of the piston ring at CR 373°, 374°, and 386° by the LST pattern of the cylinder liner that the piston ring passes on. Such increased pressures increase the film thickness and decrease the direct contact of asperities without the LST (Figures 5 and 7).

Therefore, under the high loads of power stroke after the TDC, increased film thickness due to the transient hydrodynamic pressure generates less frictional force

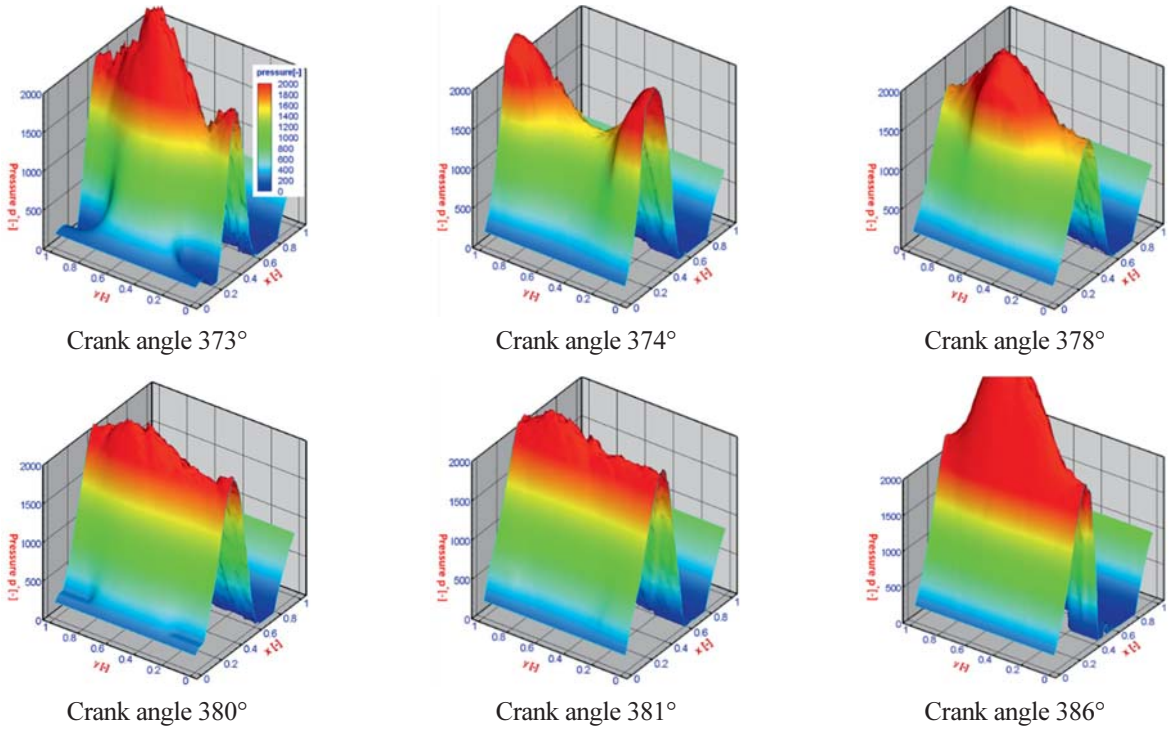

Figure 6. Variations in the hydrodynamic dimensionless pressure $p^* = (p - p_{atm})/(\mu U_{cr=1^\circ} l_{pr})$ during a cycle on LST cylinder surface (μ = 5.5 mPas, $U_{cr=1^\circ} = 0.3174 m/s$, l_{pr} = 1.2 mm) at 3000 rpm under full load.

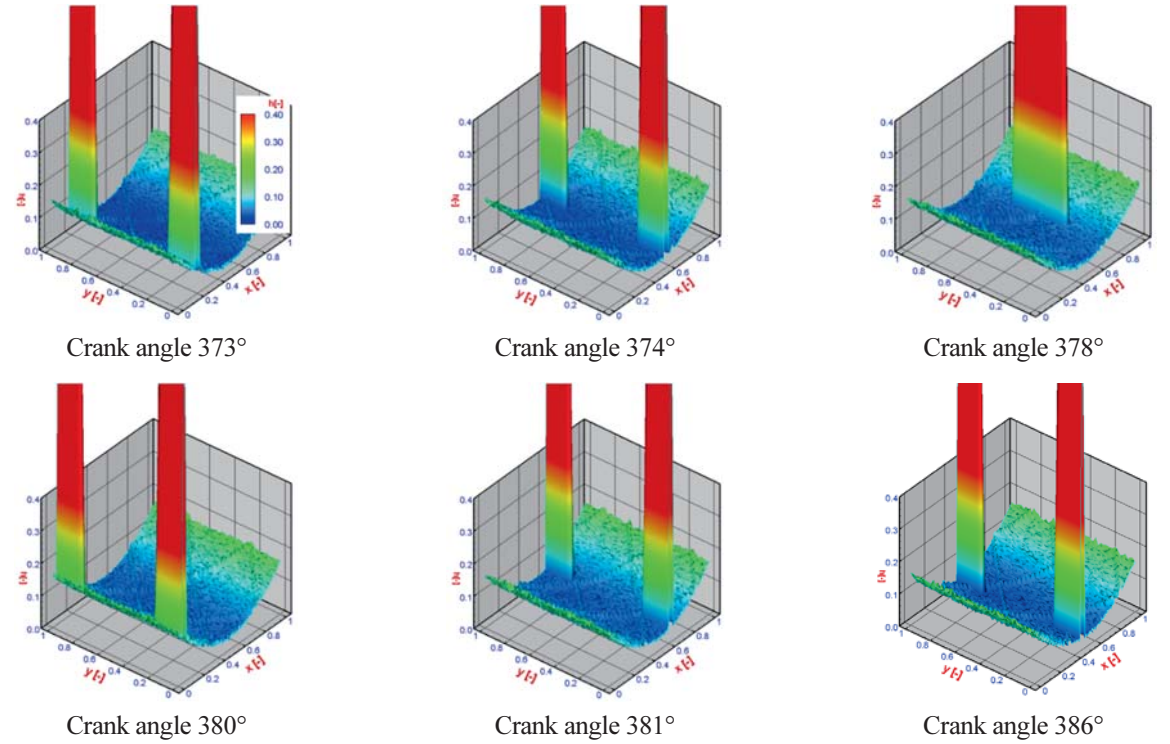

Figure 7. Variations in the hydrodynamic dimensionless lubrication film $h^* = h/h_{max}$ during a cycle on LST cylinder surface (h_{max} = *LST depth* + *honing ridge depth* + R_a) at 3000 rpm under full load.

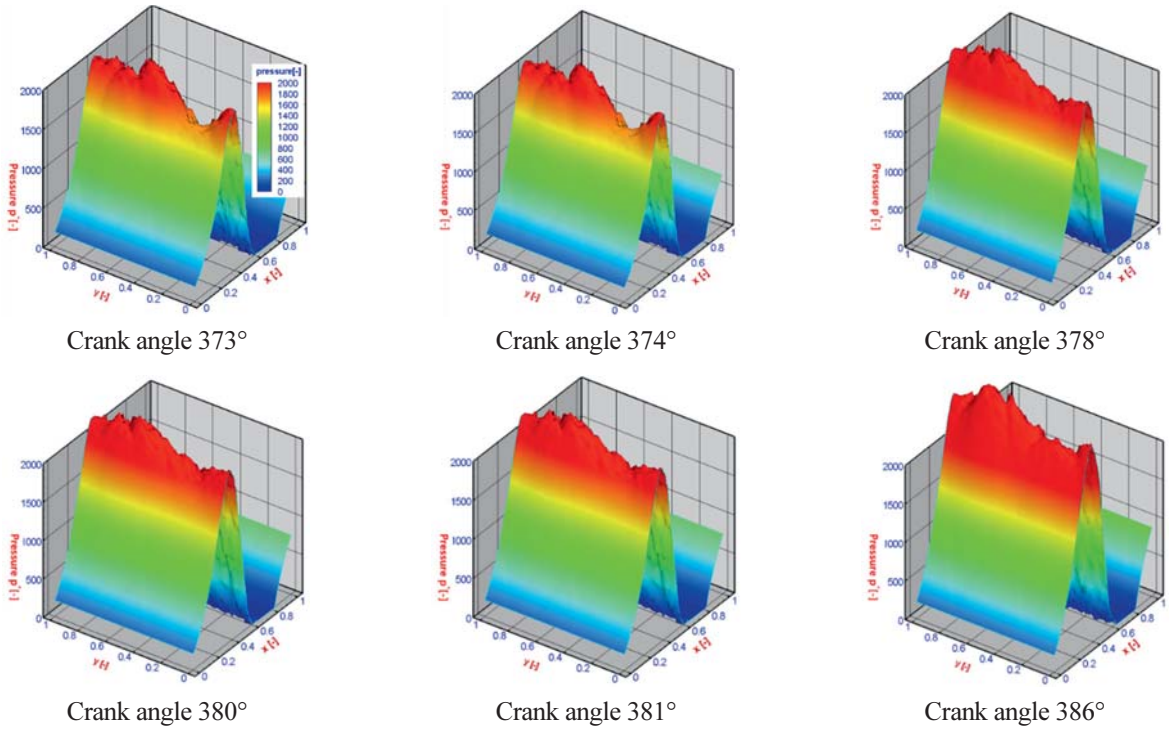

Figure 8. Variations in the hydrodynamic dimensionless pressure $p^* = (p - p_{atm})/(\mu U_{cr=1^\circ} l_{pr})$ during a cycle on smooth cylinder surface (μ = 5.5 mPas, $U_{cr=1^\circ} = 0.3174 m/s$, l_{pr} = 1.2 mm) at 3000 rpm under full load.

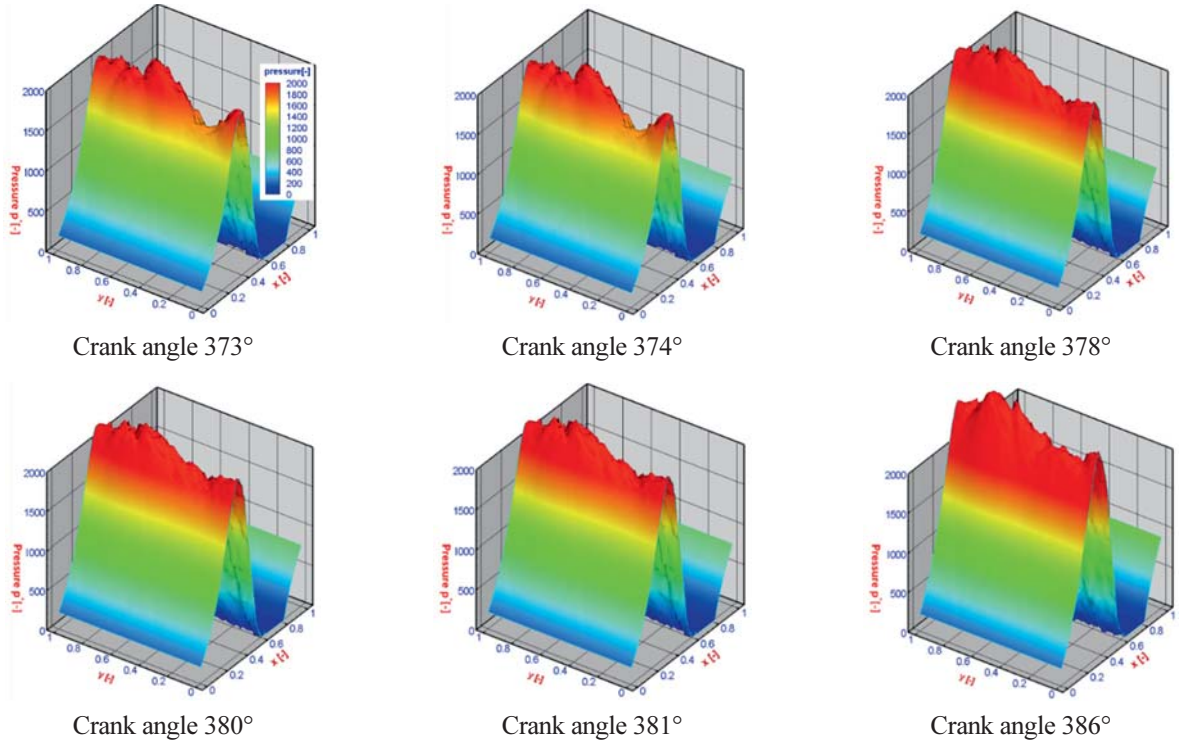

Figure 9. Variations in the hydrodynamic dimensionless lubrication film $h^* = h/h_{max}$ during a cycle on honing smooth cylinder surface (h_{max} = *LST depth* + *honing ridge depth* + R_a) at 3000 rpm under full load.

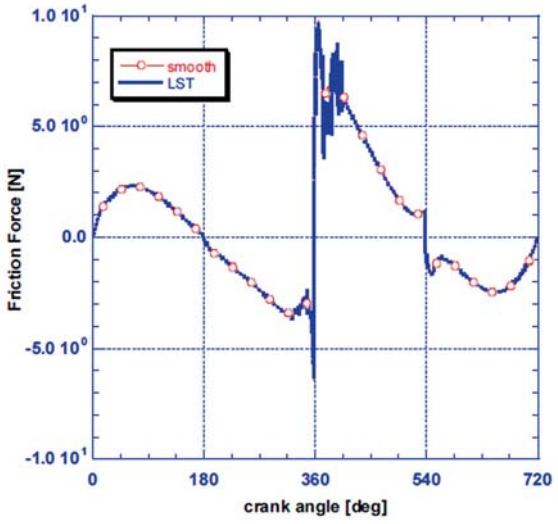

(a) Frictional force during a cycle

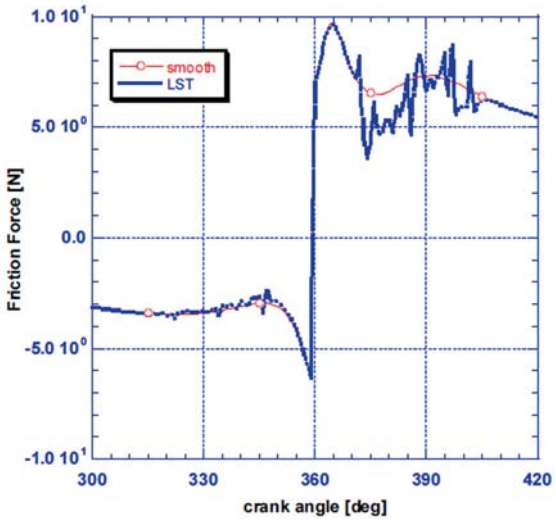

(b) Frictional force during selected crank angle range

Figure 10 (a) Variations in the friction force during a cycle and (b) Selected crank angle range during power stroke between smooth and LST-patterned cylinder surface at 3000 rpm under full load.

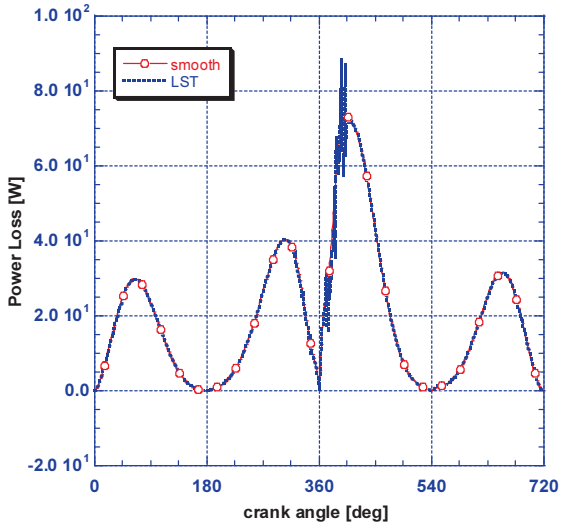

(a) Frictional power loss during a cycle

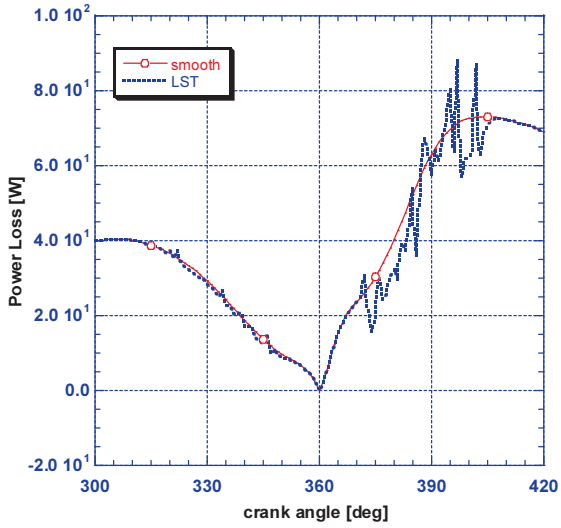

(b) Frictional power loss during selected crank angle range

Figure 11. (a) Variations in the frictional power losses during a cycle between smooth and LST-patterned cylinder surface at 3000 rpm under full load; (b) Frictional power loss during selected crank angle range.

(Figure 10), especially in the LST region of CR 370 ~ 405°. This is also due to less direct surface contact at high loads. This type of mechanism reduces the frictional force and frictional power loss (Figure 11). The total reduction in the friction force and power loss is approximately 8.19 % and 2.0 %, respectively, for the LST patterns on the cylinder liner in this computation. The LST on the cylinder liner is usually used for both frictional loss reduction and wear resistance. This work focuses on frictional performance by forming a transient lubrication film with the LST pattern on the stationary surface of the cylinder liner.

6. CONCLUSION

In this work, transient hydrodynamic lubrication behaviors on the LST-patterned cylinder liner were analyzed to investigate how friction losses can be reduced. The LST was made on a location a little distant from the TDC, where the contact behavior of the piston top ring is the most severe to have large applied load and contact velocity reversals. LST pattern is made in some part of the full stroke, because it costs too much to make LST pattern all through the stroke.

The computational results in this work show that the

minimum film thickness of the LST-patterned surface (LST surface) is thicker than that of the honing surface (smooth surface). Frictional loss can be reduced with the LST around the TDC location during the power stroke period of a high load and a slow reversal speed with the thicker film thickness. The power loss attributed to the production of friction force and contact velocity around the TDC area seems to be lower than the expected value. This phenomenon is the reason that contact velocity is very low because of the reversal contact velocity of the piston ring at the TDC location. Therefore, it reflects most of the friction force in each case between the surfaces of the LST patterned with the honing surface and the honing surface only. The thicker film with the LST-patterned surface around the TDC location can be expected to provide less wear damages by separating the contact surfaces between the piston ring and the cylinder liner.

The differences in the transient film thickness between the LST patterned with the honing surface and the surface processed with honing only can be found by applying the moving boundary conditions that depict the movement of the piston ring on the stationary patterned cylinder surface. With the computational method, transient hydrodynamic lubrication behaviors by the LST pattern on the stationary surface enhance the film thickness, thereby the load capacity of hydrodynamic pressures. In the computation, a contact reversal behavior around the TDC location under the most undergoing loading conditions is also considered. The thick film on the LST-patterned surface reduces the possibility of the direct contact between the piston ring and cylinder liner surfaces, which leads to less friction force and power loss.

ACKNOWLEDGEMENT–This work was supported by the Basic Science Program through the National Research Foundation (NRF), Grant No.: 2018R1D1A1B07043950 & BK21(5199990814084).

REFERENCES

Akalin, O. and Newaz, G. M. (2001). Piston ring-cylinder bore friction modeling in mixed lubrication regime: Part I—Analytical results. *J. Tribology* **123**, **1**, 211–218.

Carden, P., Bell, D., Priest, M. and Barrell, D. (2006). Piston assembly friction losses: Comparison of measured and predicted data. *SAE Paper No.* 2006-01-0426.

Chen, H. and Tian, T. (2008). The influences of cylinder liner honing patterns and oil control ring design parameters on the interaction between the twinland oil control ring and the cylinder liner in internal combustion engines. *SAE Paper No.* 2008-01-1614.

Checo, H. M., Ausas, R. F., Jai, M., Cadalen, J. P., Choukroun, F. and Buscaglia G. C. (2014). Moving textures: Simulation of a ring sliding on a textured liner. *Tribology Int*., **72**, 131–142.

Chong, W. W. F., Teodorescu, M. and Vaughan, N. D. (2011). Cavitation induced starvation for piston-ring/liner tribological conjunction. *Tribology Int.* **44**, **4**, 483–497.

Etsion, I. and Sher, E. (2009). Improving fuel efficiency with laser surface textured piston rings. *Tribology Int.* **42**, **4**, 542–547.

Gadeschi, G. B., Backhaus, K. and Knoll, G. (2012). Numerical analysis of laser-textured piston-rings in the hydrodynamic lubrication regime. *J. Tribology* **134**, **4**, 041702.

Greenwood, J. A. and Tripp, J. H. (1970). The contact of two nominally flat rough surface. *Proc. Institution of Mechanical Engineers* **185**, **1**, 625–633.

Hu, Y., Meng, X. and Xie, Y. (2018). A new efficient flow continuity lubrication model for the piston ring-pack with consideration of oil storage of the cross-hatched texture. *Tribology Int*., **119**, 443–463.

Jocsak, J., Li, Y., Tian, T. and Wong, V. W. (2006). Modeling and optimizing honing texture for reduced friction in internal combustion engines. *SAE Trans*., 335–347.

Knopf, M., Eiglmeier, C. and Merker, G. P. (1998). Calculation of unsteady hydrodynamic lubrication and surface contact at the piston-ring/cylinder-liner interface. *SAE Paper No.* 981402.

Kong, J. and Jang, S. (2020). Temperature analysis of wet clutch surfaces during clutch engagement processes based on friction pad patterns. *Int. J. Automotive Technology* **21**, **4**, 813-822.

Krupka, I., Hartl, M., Zimmerman, M., Houska, P. and Jang, S. (2011). Effect of surface texturing on elastohydrodynamically lubricated contact under transient speed conditions. *Tribology Int.* **44**, **10**, 1144–1150.

Li, Y., Chen, H. and Tian, T. (2008). A deterministic model for lubricant transport within complex geometry under sliding contact and its application in the interaction between the oil control ring and rough liner in internal combustion engines. *SAE Paper No.* 2008-01-1615.

Liu, C., Lu, Y., Zhang, Y., Li, S., Kang, J. and Müller, N. (2019). Numerical study on the tribological performance of ring/liner system with consideration of oil transport. *J. Tribology* **141**, **1**, 011701.

Ma, M. T., Sherrington, I. and Smith, E. H. (1996). Implementation of an algorithm to model the starved lubrication of a piston ring in distorted bores: Prediction of oil flow and onset of gas blow-by. *J. Engineering Tribology* **210**, **1**, 29–44.

Mezghani, S., Demirci, I., Yousfi, M. and El Mansori, M. (2013). Mutual influence of crosshatch angle and superficial roughness of honed surfaces on friction in ring-pack tribo-system. *Tribology Int*., **66**, 54–59.

Morris, N., Rahmani, R., Rahnejat, H., King, P. D. and Howell-Smith, S. (2016). A numerical model to study the role of surface textures at top dead center reversal in the piston ring to cylinder liner contact. *J. Tribology* **138**, **2**, 021703.

Patir, N. and Cheng, H. S. (1979). Application of average flow model to lubrication between rough sliding surfaces. *J Tribology* **101**, **2**, 220–229.

Turnbull, R., Dolatabadi, N., Rahmani, R. and Rahnejat, H. (2020). An assessment of gas power leakage and frictional losses from the top compression ring of internal combustion engines. *Tribology Int*., **142**, 105991.

Usman, A. and Park, C. W. (2017). Numerical investigation of tribological performance in mixed lubrication of textured piston ring-liner conjunction with a non-circular cylinder bore. *Tribology Int.* **105**, 148–157.

Vlădescu, S., Olver, A., Pegg, I. and Reddyhoff, T. (2015). The effects of surface texture in reciprocating contacts – An experimental study. *Tribology Int*., **82**, 28–42.

Vlădescu, S. C., Ciniero, A., Tufail, K., Gangopadhyay, A. and Reddyhoff, T. (2017), Looking into a laser textured piston ring-liner contact. *Tribology Int*., **115**, 140–153.

Zhan, J. and Yan, M. (2012). Investigation on dimples distribution angle in laser texturing of cylinder–piston ring system. *Tribology Trans.* **55**, **5**, 693–697.